

BROADBAND SUBSTRATE INTEGRATED COAXIAL LINE TO CBCPW TRANSITION FOR RAT-RACE COUPLERS AND DUAL-BAND COUPLERS DESIGN

Qiang Liu¹, Yuanan Liu¹, Yongle Wu^{1, 2, *}, Shulan Li¹,
Cuiping Yu¹, and Ming Su¹

¹School of Electronic Engineering, Beijing University of Posts and Telecommunications, Beijing 100876, China

²State Key Laboratory of Millimeter Waves, Southeast University, Nanjing 210096, China

Abstract—In this paper, broadband transitions from substrate integrated coaxial line (SICL) to a conductor-backed coplanar waveguide (CBCPW) are proposed and designed. Measurement results show that the insertion loss and return loss are better than -0.5 dB and -10 dB, respectively from 0 to 13 GHz. Then, for verifying the performance of SICL and the validity of SICL transition design, a 3 dB SICL rat-race coupler operating at 2.3 GHz is designed, fabricated, and measured. Compared with the conventional microstrip line coupler, this SICL coupler maintains good performance but with a remarkable 24% reduction in size. At last, a 10 dB dual-band coupled SICL coupler operating at 2.4/5.8 GHz is proposed, and the measured results agree well with the schematic and electromagnetic simulated results. The measured results demonstrate that the fabricated bandwidths are 30% and 12.8%, the $|S_{31}|$ are -10.1 dB and -10.3 dB, the directivities are 18 dB and 20 dB at the low (2.4 GHz) and high (5.8 GHz) operating frequencies, respectively. Compare with the dual-band coupled microstrip line coupler, performance of the dual-band coupled SICL coupler is enhanced.

1. INTRODUCTION

Substrate-integrated technology (SIT) includes the substrate integrated waveguide (SIW) and the substrate integrated coaxial line (SICL) represents an emerging and very promising candidate for the

Received 19 November 2012, Accepted 14 December 2012, Scheduled 21 December 2012

* Corresponding author: Yongle Wu (wuyongle138@gmail.com).

development of components and circuits operating in the microwave and millimeter-wave or terahertz region [1–9]. SIW structures are fabricated by two rows of conducting cylinders in a dielectric substrate that connects two parallel metal plates, and permit the implementation of classical rectangular waveguide in planar form [1]. SIW have many advantages, including easy fabrication and low cost compared with conventional metallic rectangular waveguide [2, 3]. However, the fundamental mode TE_{10} of SIW has dispersion characteristic, and it's not wise to use SIW in ultra-wideband systems. Moreover, the size of the SIW is still large owing to its TE_{10} cutoff wavelength property, especially at low frequencies. SICL is a shielded planar coaxial transmission line, comprising a conductive stripline sandwiched between the two grounded dielectric layers and side-limited by two rows of metallic via holes [4]. At first, SICL have the features of high Q , high power capability, low cost and ease of integration with other passive or active components [5]. Secondly, SICL is nearly shielded due to its two rows of metallic via holes. Because of the no-dispersive fundamental mode TEM, SICL has a broadband of single-mode operation for ultra-wideband microwave components design [6]. The highest frequency of the SICL single-mode operation bandwidth equals to the cut-off frequency of the first upper mode TE_{10} , which can be adjusted by changing the distance between SICL two rows of metallic via holes [5, 8]. Finally, the guided wavelength of TEM mode equals to the wavelength in dielectric, and SICL components can be fabricated with a reduction in size compared with SIW or microstrip line components [9]. The characteristic impedance Z_0 of the TEM mode is frequency independent, and its value can be adjusted expediently by playing with the ratio between the height of the dielectric substrate and the width of the inner conductor in the design process [4].

At present, many papers about SIW transitions have been published. SIW transitions between different layers are presented in [10], and broadband SIW-to-CBCPW transitions and ultra-wideband SIW-to-CPW are proposed in [11–13] and [14] respectively. Moreover, there are many SIW passive and active components have been studied, such as SIW filters [15–17], antenna [18], triplexer [19], oscillator [20], and so on. However, there are *a few of* papers to report SICL broadband transitions and components, and *not any papers* to propose SICL rat-race coupler and dual-band coupled SICL coupler to our best knowledge. In this paper, a novel compact SICL-to-CBCPW transition with broadband operation is proposed and designed. Since the SICL has the advantage of the no-dispersive fundamental mode TEM, and which is very suitable applying to the high performance and miniaturization design of microwave devices. In

Section 3, the application of SICL-to-CBCPW transition to the SICL 3 dB rat-race coupler for maintaining good performance and reduction in size was discussed. Compared with a conventional transmission line, a coupled line has advantages, such as compact size, flexible design parameters, and so on. There are much research has been investigated to dual-band RF passive and active components based on coupled microstrip line, such as power dividers [21–24], filters [25, 26], coupled-line couplers [27], and power amplifier [28]. However, the electromagnetic simulation results and the measured responses do not perfectly match to those of the ideal schematic circuit at the high frequency band that due to the unequal even-and odd-mode velocities in microstrip coupled lines. Compare with the microstrip line or other quasi-TEM transmission lines, SICL has the advantage of the no-dispersive fundamental mode TEM, and which is very suitable for applying to the design of microwave devices that based on coupled-line structures. Moreover, the coupled SICL can enhance the directivity of the coupler with coupled-line structure due to the equal even-and odd-mode velocities in it. In Section 4, a dual-band coupled SICL directional coupler operating at 2.4/5.8 GHz is proposed, and the measured results agree well with the schematic and electromagnetic simulated results.

2. SICL-TO-CBCPW TRANSITION

2.1. SICL-to-CBCPW Transition Design

The 3D view and the layout of the back-to-back SICL-to-CBCPW transition are shown in Figure 1 and Figure 2 respectively. The proposed structure is composed of three parts I, II, III as shown in Figure 2. The CBCPW at part I propagates quasi-TEM mode, and its characteristic impedance is determined by the thickness H of the dielectric substrate, the width W_1 of the middle conductor and the width W_2 of the slit jointly. The SICL at part III propagates TEM mode, and its characteristic impedance can be adjusted by changing the ratio between the height H of the substrate and the width W_3 of the inner conductor. The diameter of via hole is D and the period is T , and the distance between the two rows of via holes is A in Figure 2. The SICL and the CBCPW was connected by a blind hole in the transition region at part II, which diameter equals to W_3 and height is h . In order to achieve electromagnetic field convert gradually, semicircular conductor with diameter W_1 was utilized, and the width of the space between this semicircular conductor and the ground conductor on the top layer was increased from the minimum value $0.5(W_2 - W_1)$ at the CBCPW end to the parameter gap gradually in Figure 2. The

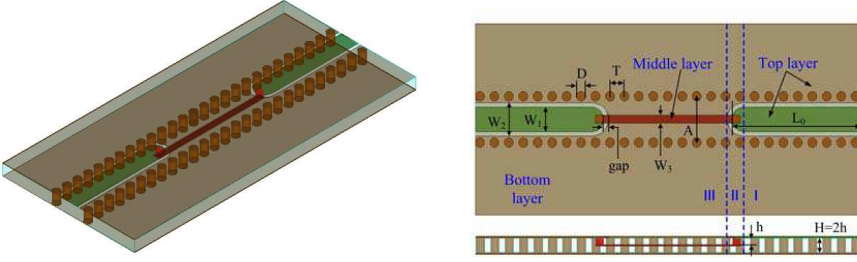


Figure 1. The 3D view of the back-to-back SICL-to-CBCPW transition.

Figure 2. Layout of the back-to-back SICL-to-CBCPW transition.

performance of this transition can be adjusted by changing the value of the gap.

This back-to-back SICL-to-CBCPW transition model shown in Figure 1 was simulated and optimized by using the Ansys High Frequency Structural Simulator (HFSS), where the thickness of the dielectric substrate is $H = 1.634$ mm with dielectric constant $\epsilon_r = 3.48$. The parameters for the $Z_0 = 50\ \Omega$ CBCPW is $W_1 = 2.5$ mm, $W_2 = 3.4$ mm, $L_0 = 14$ mm and for the $Z_0 = 50\ \Omega$ SICL is $W_3 = 0.86$ mm. The parameters $D = 1$ mm and $T = 1.6$ mm, which are usually imposed by technological constraints. $A = 5$ mm has been proven to control the single-mode bandwidth from 0 to $f_{TE_{10}} = 18.52$ GHz, where $f_{TE_{10}} = 18.52$ GHz is the cut-off frequency of the TE_{10} mode for this SICL [4]. The optimized parameter gap = 0.6 mm was obtained with the aid of HFSS.

2.2. Experiment Results

The back-to-back SICL-to-CBCPW transition was fabricated on a bilayer substrate Rogers 4350B with $\epsilon_r = 3.48$, and the thickness of each layer is $h = 0.762$ mm with loss tangent of 0.004. Figure 3 shows this back-to-back transition structure with SMA connectors. The S -parameters of the fabricated back-to-back transitions are measured by Agilent PNA N5230C, and the simulation and measurement results of the insertion loss $|S_{21}|$ and the return loss $|S_{11}|$ are shown in Figure 4. The measured S parameter of the microstrip line with the same length and same SMA connectors was also shown for comparison in Figure 4.

See from Figure 4, the measured return loss of the back-to-back SICL-to-CBCPW transition with SMA connector is less than -10 dB and the insertion loss is better than -1.72 dB from 0 to 13 GHz. The performance of the back-to-back transitions was degraded

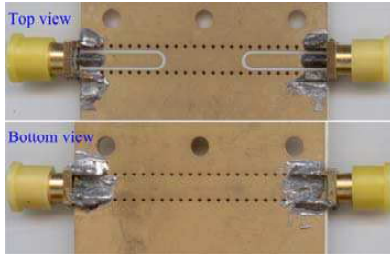


Figure 3. Photograph of the fabricated back-to-back SICL-to-CBCPW transition.

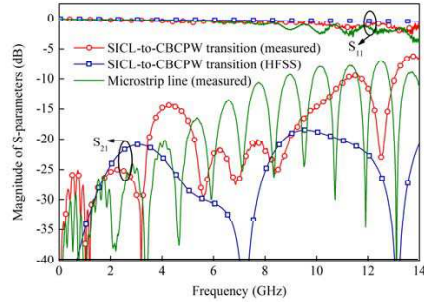


Figure 4. Insertion loss and return loss of the back-to-back SICL-to-CBCPW transition and the microstrip line.

around 4.2 GHz due to the resonant phenomena in the CBCPW [29]. Moreover, the measured insertion loss of the microstrip line with the same length and same SMA connectors are -1.98 dB and -2.23 dB at 9 GHz and 13 GHz respectively, and the measured insertion loss of each SMA connector is worse than -0.5 dB at least in the frequency range from 9 GHz to 13 GHz. After eliminating the insertion loss caused by the two SMA connectors, the insertion loss is better than -0.5 dB for a single SICL-to-CBCPW transition from 0 to 13 GHz.

3. SICL 3-dB RAT-RACE COUPLER

To verify the performance of SICL and the validity of SICL transition design, the SICL 3 dB rat-race coupler with center frequency $f_0 = 2.3$ GHz shown in Figure 5 was designed and simulated with the aid of the HFSS. The parameters $W_4 = 0.4$ mm for $Z = 70.7 \Omega$ SICL and $W_5 = 0.86$ mm for $Z_0 = 50 \Omega$ SICL, $R_0 = 16.7$ mm, $R_1 = 14.2$ mm, $R_2 = 19.2$ mm, and $H = 1.634$ mm. There are four SICL-to-CBCPW transitions describing in Section 2 are used for testing the SICL 3 dB rat-race coupler. Port 2 is the sum port (Σ) and Port 4 is difference port (Δ). A signal excited on Port 2 will be evenly split into two in-phase signals at Port 1 and Port 3, and Port 4 will be isolated. If the input is applied to Port 4, it will be equally split into two out-of-phase signals at Port 1 and Port 3, and Port 2 will be isolated [30]. The perimeter of the conductor annulus with radius R_0 in the middle layer equals to $1.5\lambda_g$, and $\lambda_g = 70$ mm is the guide wavelength for the SICL at 2.3 GHz. However, the guide wavelength of microstrip line

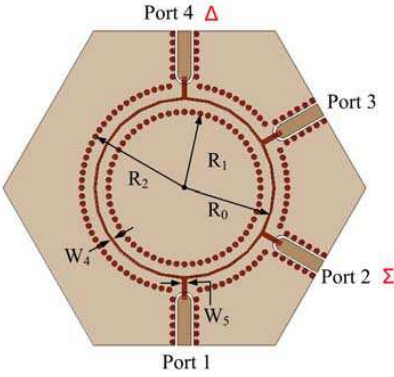


Figure 5. Layout of the SICL 3 dB rat-race coupler.

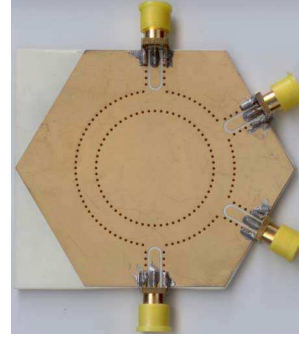


Figure 6. Photograph of the fabricated SICL 3 dB rat-race coupler.

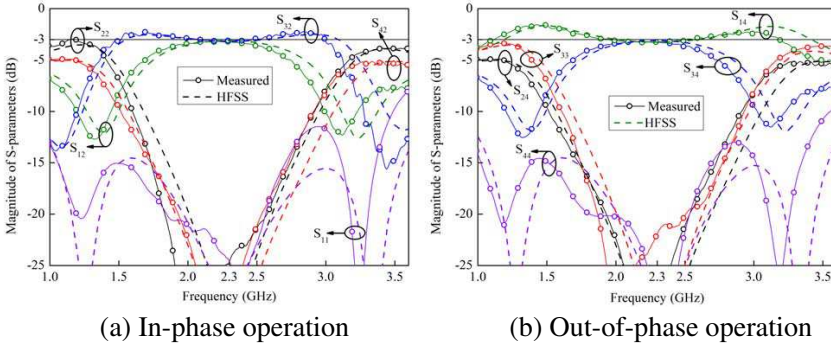


Figure 7. Magnitude of S -parameters of the SICL 3 dB rat-race coupler.

is $\lambda_g = 78$ mm for same operation frequency and dielectric substrate. Therefore, compare with microstrip line coupler, this SICL coupler has 24% reduction in size.

The 3 dB rat-race coupler was fabricated on a bilayer substrate Rogers 4350B with $\epsilon_r = 3.48$, and the thickness of each layer is $h = 0.762$ mm with loss tangent of 0.004. The S -parameters of the fabricated coupler with four SMA connectors shown in Figure 6 were measured by Agilent PNA N5230C. Figure 7 and Figure 8 illustrate the amplitude and phase properties of the S -parameters respectively. Figure 7(a) and Figure 8(a) show the amplitude and in-phase properties as signal applied to Port 2 (Σ). Figure 7(b)

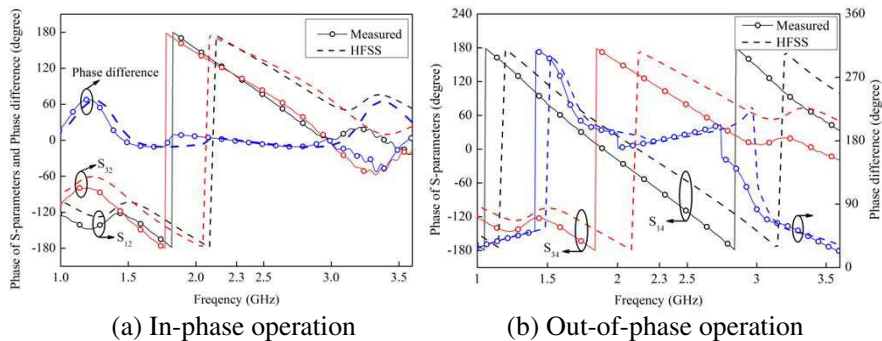


Figure 8. Phase of S -parameters and phase difference of the SICL 3 dB rat-race coupler.

and Figure 8(b) show the amplitude and out-of-phase properties as signal applied to Port 4 (Δ). The measurement result is in good agreement with the simulation result except for 50 MHz central frequency deviation, which may be attributed to the fabrication tolerance. From Figure 7 and Figure 8, it can be seen the insertion loss is -3.2 dB, the return loss and isolation are better than -25 dB, the phase difference is 0.2° for the case of in-phase operation and 180.4° for the out-of-phase operation at 2.3 GHz. In the range of 1.75 to 2.65 GHz and fractional bandwidth 39%, the insertion loss $|S_{32}|$, $|S_{12}|$, $|S_{34}|$ and $|S_{14}|$ are better than -3.2 dB ± 1 dB, the return loss $|S_{11}|$, $|S_{22}|$, $|S_{44}|$, $|S_{33}|$ and the isolation S_{42} are better than -17 dB in band. The maximum of phase difference is $\pm 10^\circ$ for in-phase operation and $180^\circ \pm 10^\circ$ for out-of-phase operation, respectively. Moreover, the differential phase 48° between the measurement result and the simulation result in Figure 8 were due to the four SMA connectors, which was employed in the measurement but not considered in the simulation.

4. DUAL-BAND COUPLED SICL COUPLER

In order to compare the performances of the coupled SICL and the coupled microstrip line, a dual-band coupled SICL 10-dB coupler operating at 2.4/5.8 GHz in Figure 9 was designed and fabricated in this Section. The design parameters of the dual-band coupled SICL 10-dB coupler can be obtained as follow formulas [27] for the system characteristic impedance $Z_0 = 50 \Omega$:

$$\begin{cases} \frac{\theta_2}{\theta_1} = \frac{f_2}{f_1} \\ \theta_1 = \pi - \theta_2 \end{cases}, \tag{1}$$

$$\begin{cases} Z_{0e2} = \frac{Z_0 \sqrt{\frac{1+C}{1-C}}}{\sin \theta}; \\ Z_{0o2} = \frac{Z_0 \sqrt{\frac{1-C}{1+C}}}{\sin \theta}; \\ \frac{Z_{0e1}}{Z_{0e2}} = \frac{Z_{0o1}}{Z_{0o2}} = k = \tan^2 \theta; \\ \theta = \theta_1 \text{ or } \theta_2. \end{cases} \tag{2}$$

where Z_{0e1} , Z_{0o1} , Z_{0e2} , Z_{0o2} are even- and odd-mode characteristic impedances of the two coupled SICL section, respectively. C is the coupling coefficient, f_1/f_2 the two operation frequency 2.4/5.8 GHz, and θ_1 and θ_2 are electrical length of the two coupled SICL section for f_1 and f_2 . After substitute f_1 and f_2 in formula (1) and (2) above. The parameters of the dual-band coupled SICL 10-dB coupler with operating frequency 2.4/5.8 GHz are attained $Z_{0e1} = 150 \Omega$, $Z_{0o1} = 78 \Omega$, $Z_{0e2} = 87 \Omega$, $Z_{0o2} = 45 \Omega$, $\theta_1 = 52.7^\circ$, $\theta_2 = 127.3^\circ$. Then, the coupler showing in Figure 9 was designed with the aid of HFSS. Because the almost identical electromagnetic field of the coupled SICL and the coupled strip-line, and the dimensions of the coupled SICL coupler in Figure 9 $K_1 = 0.1 \text{ mm}$, $S_1 = 0.43 \text{ mm}$, $K_2 = 0.44 \text{ mm}$, $S_2 = 0.23 \text{ mm}$, $L_1 = L_2 = 9.81 \text{ mm}$ are obtained. Four SICL-to-CBCPW transitions describing in Section 2 are used for the dual-band coupled SICL coupler test.

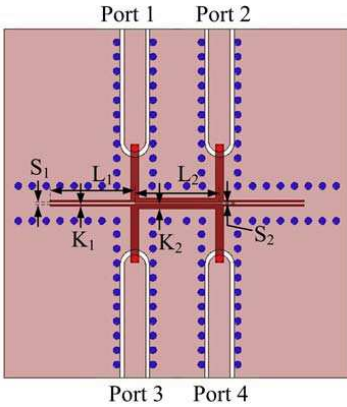


Figure 9. Layout of the dual-band coupled SICL 10-dB coupler.

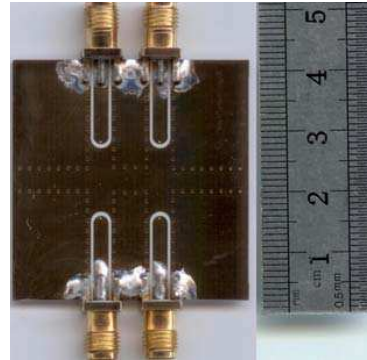


Figure 10. Photograph of the fabricated dual-band coupled SICL 10-dB coupler.

The coupler is fabricated on a bilayer substrate Rogers 4350B with $\epsilon_r = 3.48$, and the thickness of each layer is $h = 0.762$ mm with loss tangent of 0.004. The S -parameters of the fabricated dual-band coupled SICL 10-dB coupler with four SMA connectors show in Figure 10 are tested with Agilent PNA N5230C. Figure 11 and Figure 12 illustrate the measured, schematic, and HFSS simulated S -parameter results of the dual-band coupled SICL 10-dB coupler. The measured results agree well with the schematic and HFSS simulated results except $|S_{11}|$ response at the higher frequency band due to the T -junction discontinuous. See from Figure 11(a), the measured $|S_{31}|$ are -10.1 dB and -10.3 dB, and $|S_{21}|$ are -0.73 dB and -1.05 dB at 2.4/5.8 GHz respectively. In Figure 11(b), the measured $|S_{11}|$ are -33 dB and -17 dB, and $|S_{41}|$ are -28 dB and -30 dB at 2.4/5.8 GHz respectively. The maximum of $|S_{31}|$ is -9.95 dB and the fabricated

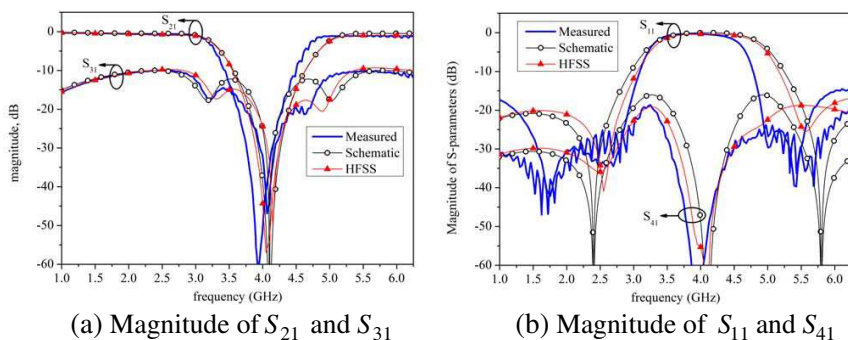


Figure 11. Magnitude of S -parameters of the dual-band coupled SICL 10-dB coupler.

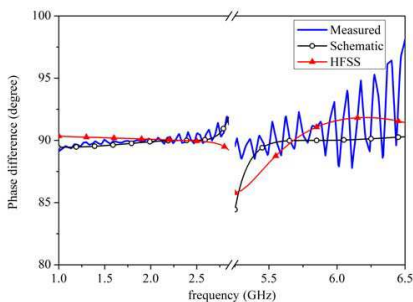


Figure 12. Phase difference between the two output ports of the dual-band coupled SICL 10-dB coupler.

bandwidths of $|S_{31}| > -10.5$ dB at the two operating frequencies are 2.08–2.80 GHz and 5.18–5.92 GHz respectively, and the fractional bandwidths are 30% and 12.8% accordingly. As seen from Figure 12, the phase difference between the port 2 and port 3 are $90 \mp 2.3^\circ$ in band. It should be mentioned that the directivities $|S_{31}| - |S_{41}|$ are 18 dB and 20 dB at 2.4/5.8 GHz respectively. Compare with the directivities of the dual-band coupled microstrip line 2.4/5.8 GHz coupler are 13 dB and 6 dB we are measured, the directivities of the dual-band coupled SICL coupler are 5 dB and 14 dB better at 2.4/5.8 GHz respectively.

5. CONCLUSIONS

In this paper, the broadband SICL-to-CBCPW transition was proposed, designed, and fabricated. The measurement results show that the $|S_{21}|$ is more than -0.5 dB and the $|S_{11}|$ is better than -10 dB for a SICL-to-CBCPW transition from 0 to 13 GHz. Then, the 3 dB rat-race coupler with performance enhancement by SICL is proposed and measured. The measurement results show that the insertion loss is -3.2 dB, the return loss and the isolation are better than -25 dB, the differential phase is 0.2° for the case of in-phase operation and 180.4° for the out-of-phase operation at the center frequency. In the range of 1.75 to 2.65 GHz, the maximum of output amplitude imbalance is better than -3.2 dB ± 1 dB with fractional bandwidth 39%, the return loss and the isolation are better than -17 dB, and the maximum of output phase imbalance is $\pm 10^\circ$ in band. Compare with microstrip line coupler, this SICL coupler has 24% reduction in size. At last, a dual-band coupled SICL coupler operating at 2.4/5.8 GHz is designed, and the measured results agree well with the schematic and HFSS simulated results. The coupler can provide better performance at dual operation frequency bands as compared to its dual-band coupled microstrip line coupler counterpart. Especially, the directivities of the dual-band coupled SICL coupler are 5 dB and 14 dB better at 2.4 GHz and 5.8 GHz, respectively.

ACKNOWLEDGMENT

This work was supported in part by the National Natural Science Foundation of China (No. 61001060, No. 61201025, and No. 61201027), the Fundamental Research Funds for the Central Universities (No. 2012RC0301 and No. 2012TX02), and Open Project of the State Key Laboratory of Millimeter Waves (Grant No. K201316).

REFERENCES

1. Deslandes, D. and K. Wu, "Integrated microstrip and rectangular waveguide in planar form," *IEEE Microw. Wireless Compon. Lett.*, Vol. 11, 68–70, 2001.
2. Wu, K., "Substrate integrated circuits (SICs) for low-cost high-density integration of millimeter-wave wireless systems," *IEEE Radio and Wireless Symp.*, 683–686, 2008.
3. Bozzi, M., A. Georgiadis, and K. Wu, "Review of substrate-integrated waveguide circuits and antennas," *IET Microwaves, Antennas & Propagation*, Vol. 5, 909–920, 2011.
4. Gatti, F., M. Bozzi, L. Perregrini, K. Wu, and R. G. Bosisio, "A novel substrate integrated coaxial line (SICL) for wide-band applications," *36th European Microwave Conference*, 1614–1617, 2006.
5. Gatti, F., M. Bozzi, L. Perregrini, K. Wu, and R. G. Bosisio, "A new wide-band six-port junction based on substrate integrated coaxial line (SICL) technology," *IEEE Mediterranean Electrotechnical Conference*, 367–370, 2006.
6. Zhu, F., W. Hong, J.-X. Chen, and K. Wu, "Ultra-wideband single and dual baluns based on substrate integrated coaxial line technology," *IEEE Trans. Microw. Theory Tech.*, Vol. 60, No. 10, 3062–3070, 2012.
7. Zhou, Y. and S. Lucyszyn, "Modelling of reconfigurable terahertz integrated architecture (Retina) SIW structures," *Progress In Electromagnetics Research*, Vol. 105, 71–92, 2010.
8. Urbano, D., E. Arnieri, G. Cappuccino, and G. Amendola, "Simulation and timing performances of integrated waveguides for ultra-high speed interconnects," *Microwave Opt. Technol. Lett.*, Vol. 50, 666–672, 2008.
9. Liang, W. and W. Hong, "Substrate integrated coaxial line 3 dB coupler," *Electronics Letters*, Vol. 48, 35–36, 2012.
10. Song, K. and Y. Fan, "Ku-band substrate integrated waveguide transitions between layers," *Microwave Opt. Technol. Lett.*, Vol. 51, 2585–2588, 2009.
11. Deslandes, D. and K. Wu, "Analysis and design of current probe transition from grounded coplanar to substrate integrated rectangular waveguides," *IEEE Trans. Microw. Theory Tech.*, Vol. 53, 2487–2494, 2005.
12. Chen, X. P. and K. Wu, "Low-loss ultra-wideband transition between conductor-backed coplanar waveguide and substrate integrated waveguide," *IEEE MTT-S Int. Microwave Symp. Dig.*,

- 349–352, 2009.
13. Koziel, S. and S. Ogurtsov, “Design of broadband transitions for substrate integrated circuits,” *Microwave Opt. Technol. Lett.*, Vol. 53, 2942–2945, 2011.
 14. Lee, S., S. Jung, and H. Y. Lee, “Ultra-wideband CPW-to-substrate integrated waveguide transition using an elevated-CPW section,” *IEEE Microw. Wireless Compon. Lett.*, Vol. 18, 746–748, 2008.
 15. Zhang, Q. L., W. Y. Yin, S. He, and L. S. Wu, “Evanescence-mode substrate integrated waveguide (SIW) filters implemented with complementary split ring resonators,” *Progress In Electromagnetics Research*, Vol. 111, 419–432, 2011.
 16. Xu, Z. Q., Y. Shi, P. Wang, J. X. Liao, and X. B. Wei, “Substrate integrated waveguide (SIW) filter with hexagonal resonator,” *Journal of Electromagnetic Waves and Applications*, Vol. 26, Nos. 11–12, 1521–1527, 2012.
 17. Jedrzejewski, A., N. Leszczynska, L. Szydlowski, and M. Mrozowski, “Zero-pole approach to computer aided design of in-Line SIW filters with transmission zeros,” *Progress In Electromagnetics Research*, Vol. 131, 517–533, 2012.
 18. Masa-Campos, J. L., P. Rodriguez-Fernandez, M. Sierra-Pérez, and J. L. Fernandez-Jambrina, “Monopulse circularly polarized SIW slot array antenna in millimetre band,” *Journal of Electromagnetic Waves and Applications*, Vol. 25, Nos. 5–6, 857–868, 2011.
 19. Corona-Chavez, A. and T. Itoh, “Novel miniaturized triplexer using substrate integrated technology,” *Asia-Pacific Microwave Conference Proceedings*, 678–681, 2010.
 20. Liu, Y., X. H. Tang, and T. Wu, “SIW-based low phase-noise millimeter-wave planar dual-port voltage-controlled oscillator,” *Journal of Electromagnetic Waves and Applications*, Vol. 26, Nos. 8–9, 1059–1069, 2012.
 21. Li, J., Y. Wu, Y. Liu, J. Shen, S. Li, and C. Yu, “A generalized coupled-line dual-band Wilkinson power divider with extended ports,” *Progress In Electromagnetics Research*, Vol. 129, 197–214, 2012.
 22. Wu, Y., Y. Liu, and Q. Xue, “An analytical approach for a novel coupled-line dual-band Wilkinson power divider,” *IEEE Trans. Microw. Theory Tech.*, Vol. 59, No. 2, 286–294, 2011.
 23. Li, B., X. Wu, N. Yang, and W. Wu, “Dual-band equal/unequal wilkinson power dividers based on coupled-line section with short-

- circuited stub,” *Progress In Electromagnetics Research*, Vol. 111, 163–178, 2011.
24. Lin, Z. and Q.-X. Chu, “A novel approach to the design of dual-band power divider with variable power dividing ratio based on coupled-lines,” *Progress In Electromagnetics Research*, Vol. 103, 271–284, 2010.
 25. Lee, S. and Y. Lee, “A uniform coupled-line dual-band filter with different bandwidths,” *IEEE Microw. Wireless Compon. Lett.*, Vol. 20, No. 10, 545–547, 2010.
 26. Chen, X. W., L. Li, Y. Zhang, Y. Geng, and W. Zhang, “Balanced dual-band bandpass filter based on asymmetrical coupled lines,” *Electromagnetics*, Vol. 32, No. 1, 1–7, 2012.
 27. Wang, X., W.-Y. Yin, and K.-L. Wu, “A dual-band coupled-line coupler with an arbitrary coupling coefficient,” *IEEE Trans. Microw. Theory Tech.*, Vol. 60, No. 4, 945–951, 2012.
 28. Li, S., B. Tang, Y. Liu, S. Li, C. Yu, and Y. Wu, “Miniaturized dual-band matching technique based on coupled-line transformer for dual-band power amplifiers design,” *Progress In Electromagnetics Research*, Vol. 131, 195–210, 2012.
 29. Lo, W. T., C. C. Tzuang, S. T. Peng, C. C. Tien, C. C. Chang, and J. W. Huang, “Resonant phenomena in conductor-backed coplanar waveguides (CBCPW’s),” *IEEE Trans. Microw. Theory Tech.*, Vol. 41, 2099–2108, 1993.
 30. Pozar, D. M., *Microwave Engineering*, 3rd Edition, 352, Wiley, New York, 2005.